e-ISSN: 1390-5902
CEDAMAZ, Vol. XX, No. XX, pp. 48–54, Enero–Junio 2025
DOI: 10.54753/cedamaz.v15i1.2487

Optimization of SWIR Image Capture and Processing for Defect Detection in Photovoltaic Panels

Optimización de la Captura y Procesamiento de Imágenes SWIR para la Detección de Defectos en Paneles Fotovoltaicos

Franklin Gómez-López[1,*], Danny Ochoa-Correa[2] and Isabel Cabrera-Carrera[3]

[1] *Universidad de Cuenca, Facultad de Ingeniería, Cuenca, Ecuador, franklin.gomez@ucuenca.edu.ec*
[2] *Department of Electrical, Electronics and Telecommunications Engineering, Universidad de Cuenca, Cuenca, Ecuador, danny.ochoac@ucuenca.edu.ec*
[3] *Universidad de Cuenca, Facultad de Ingeniería, Cuenca, Ecuador, isabel.cabrera@ucuenca.edu.ec*
[*] *Autor para correspondencia: danny.ochoac@ucuenca.edu.ec*

Reception date of the manuscript: 24/05/2025 Acceptance date of the manuscript: DD/MM/YYYY Publication date: DD/MM/YYYY

Abstract—This work introduces a methodology for capturing and processing Short-Wave Infrared (SWIR) images aimed at identifying structural defects in photovoltaic panels. Indium Gallium Arsenide (InGaAs) sensors were used together with perspective correction, background subtraction, and contrast enhancement using the CLAHE algorithm. Experimental validation was carried out on mono- and polycrystalline PV modules using a dark chamber and controlled polarization currents, following the procedures outlined in IEC TS 60904-13. Proper configuration of capture parameters—specifically exposure time, gain, and polarization current—combined with a structured preprocessing sequence led to accurate detection of defects such as cracks, inactive zones, and discontinuities in collector bars. The proposed approach resulted in a signal-to-noise ratio (SNR) improvement of 35.3 %, enabling consistent visualization of anomalies under controlled conditions. This method is suitable for integration into preventive maintenance workflows, contributing to early fault detection and extended system availability.

Keywords—Electroluminescence, SWIR, Photovoltaic Panels, Image Processing, Preventive Maintenance

Resumen—Este trabajo presenta una metodología para la captura y procesamiento de imágenes en el rango del infrarrojo de onda corta (SWIR), orientada a la identificación de defectos estructurales en paneles fotovoltaicos. Se utilizaron sensores de Indio Galio Arseniuro (InGaAs) junto con técnicas de corrección de perspectiva, sustracción de fondo y mejora de contraste mediante el algoritmo CLAHE. La validación experimental se realizó sobre módulos fotovoltaicos mono y policristalinos, empleando una cámara oscura y corrientes de polarización controladas, siguiendo los procedimientos establecidos en la norma IEC TS 60904-13. Una configuración adecuada de los parámetros de captura—específicamente el tiempo de exposición, la ganancia y la corriente de polarización—combinada con una secuencia estructurada de preprocesamiento, permitió una detección precisa de defectos como grietas, zonas inactivas y discontinuidades en las barras colectoras. El enfoque propuesto resultó en una mejora del 35.3 % en la relación señal/ruido (SNR), lo que permitió una visualización consistente de anomalías en condiciones controladas. Esta metodología es adecuada para su integración en programas de mantenimiento preventivo, contribuyendo a la detección temprana de fallas y a una mayor disponibilidad operativa del sistema.

Palabras clave—Electroluminiscencia, SWIR, Paneles Fotovoltaicos, Procesamiento de Imágenes, Mantenimiento Preventivo

INTRODUCTION

The rapid global deployment of photovoltaic (PV) systems in both centralized and distributed configurations has intensified the need for improved monitoring and diagnostic strategies that ensure long-term system reliability and energy yield. PV modules are exposed to a wide range of environmental and operational stressors that lead to gradual degradation, including delamination, solder joint corrosion, potential-induced degradation (PID), and particularly, the formation of micro-cracks in silicon cells (Buerhop-Lutz y cols., 2018; Jordan y Kurtz, 2017; Lofstad-Lie y cols., 2024). These defects compromise the electrical continuity of current pathways, resulting in localized power loss, elevated thermal stress, and accelerated aging.

Routine inspection and preventive maintenance are essential to mitigate performance losses. However, traditional field inspection techniques such as infrared thermography and visual assessments provide limited resolution and are ineffective in detecting subsurface defects or fine-scale discontinui-

ties within the cells, especially under partial shading or early-stage degradation scenarios (Zhang y cols., 2022; Matusz-Kalász y cols., 2025). These limitations have led to a growing interest in alternative diagnostic tools that leverage non-visible spectra for enhanced fault identification.

Electroluminescence (EL) imaging has gained widespread use in PV diagnostics due to its capacity to reveal structural anomalies at the cell level. By applying a forward bias to the module, EL enables the visualization of current pathways and inactive areas through near-infrared emissions. However, conventional EL imaging using silicon-based CCD or CMOS sensors typically operates within the 300–1000 nm range, which limits its sensitivity to low-intensity emissions and restricts the contrast in cells affected by subtle mechanical or electrical degradation (Qin y cols., 2021; Redondo-Plaza y cols., 2025).

To address these limitations, imaging in the Short-Wave Infrared (SWIR) band—specifically between 900 and 1700 nm—has been explored as a more effective approach. SWIR cameras equipped with Indium Gallium Arsenide (InGaAs) sensors offer improved detection of internal cell structures and enable imaging under low-excitation conditions, facilitating defect localization with higher contrast and better penetration through encapsulant layers (Mei y cols., 2020; Li y cols., 2022). This spectral advantage becomes particularly useful in detecting faint or diffuse electroluminescent signals that arise in micro-cracked or PID-affected regions.

Nonetheless, the practical implementation of SWIR-based EL imaging poses its own challenges. Image quality depends heavily on the calibration of capture parameters such as exposure time, digital gain, and polarization current. In addition, captured images often suffer from geometric distortions, fixed-pattern noise, and uneven background illumination. To extract diagnostically relevant information, it is necessary to apply a robust preprocessing pipeline that includes background subtraction, perspective correction, and local contrast enhancement methods such as Contrast Limited Adaptive Histogram Equalization (CLAHE).

Despite the growing availability of advanced imaging techniques, there remains a limited number of studies that integrate hardware optimization with tailored image processing methods for SWIR-based EL diagnostics. Moreover, current literature often focuses on either experimental validation or post-processing algorithms in isolation, leaving a gap in holistic approaches that combine acquisition and analysis within a single workflow (Chen y cols., 2021; Rehman y cols., 2023).

This study proposes and validates a complete methodology that combines optimized SWIR image acquisition with a systematic preprocessing framework to support the early detection of structural defects in PV modules. The methodology involves the experimental configuration of polarization currents and exposure parameters, followed by the implementation of automated image corrections to improve defect visibility. The ultimate goal is to enable cost-effective, high-resolution diagnostics that support predictive maintenance and lifecycle extension of PV systems, especially in environments where standard inspection methods fall short.

Materials and Methods

Experimental Setup

Experimental evaluations were conducted at the Microgrid Laboratory of the University of Cuenca (Espinoza y cols., 2017). The image acquisition system comprised an OWL 640 M camera equipped with a 16 mm focal length lens and an InGaAs sensor. This setup enabled the capture of SWIR images in the 900–1700 nm wavelength range, which is well-suited for detecting internal structural features in crystalline silicon PV modules (Mei y cols., 2020).

The test samples included both monocrystalline and polycrystalline PV panels, selected to represent configurations commonly found in utility-scale and distributed generation systems. To induce electroluminescence emissions, a programmable Chroma DC power supply was used to apply polarization currents ranging from 2 A to 8 A.

Image acquisition was performed using the XCAP-Std software, which provided precise control over exposure time, gain, and frame rate parameters. Experimental runs were conducted to assess the influence of these parameters on image contrast, uniformity, and the visibility of structural anomalies.

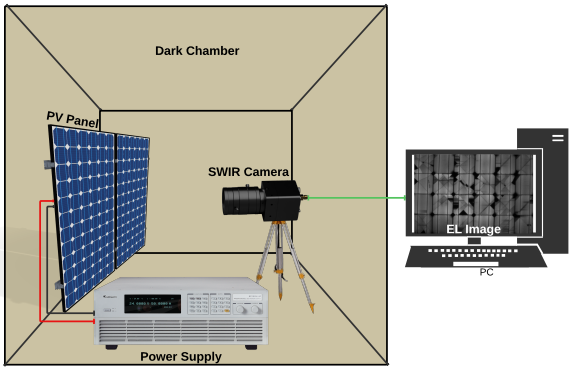

Fig. 1: Experimental setup showing the OWL 640 M camera, Chroma power supply, and PV panel under inspection.

Image Acquisition Procedure

The electrical excitation applied to the PV panels directly affects the quality and clarity of the resulting EL images. To determine an appropriate polarization current (I_{EL}), experimental tests were conducted using a Heckert Solar NeMo 60 P260 13 polycrystalline module. This panel, with an open-circuit voltage (V_{OC}) of 39.4 V and a short-circuit current (I_{SC}) of 8.97 A, was placed inside a dark chamber during acquisition. For practical purposes, V_{OC} and I_{SC} were approximated to 40 V and 9 A, respectively.

Current levels ranging from $\frac{1}{6}I_{SC}$ to I_{SC} were applied to assess their impact on image quality. Figure 2 displays EL images obtained under these varying conditions. The analysis showed that although $I_{EL} = I_{SC}$ resulted in the most intense emission, structural features could already be distinguished from $\frac{1}{2}I_{SC}$, allowing the use of lower excitation while limiting thermal stress on the panel.

For preventive maintenance applications, using a current equal to or greater than $\frac{3}{6}I_{SC}$ was found to provide sufficient EL signal intensity without introducing excessive thermal stress on the module. This observation is consistent with the

e-ISSN: 1390-5902
CEDAMAZ, Vol. XX, No. XX, pp. 48–54, Enero–Junio 2025
DOI: 10.54753/cedamaz.v15i1.2487

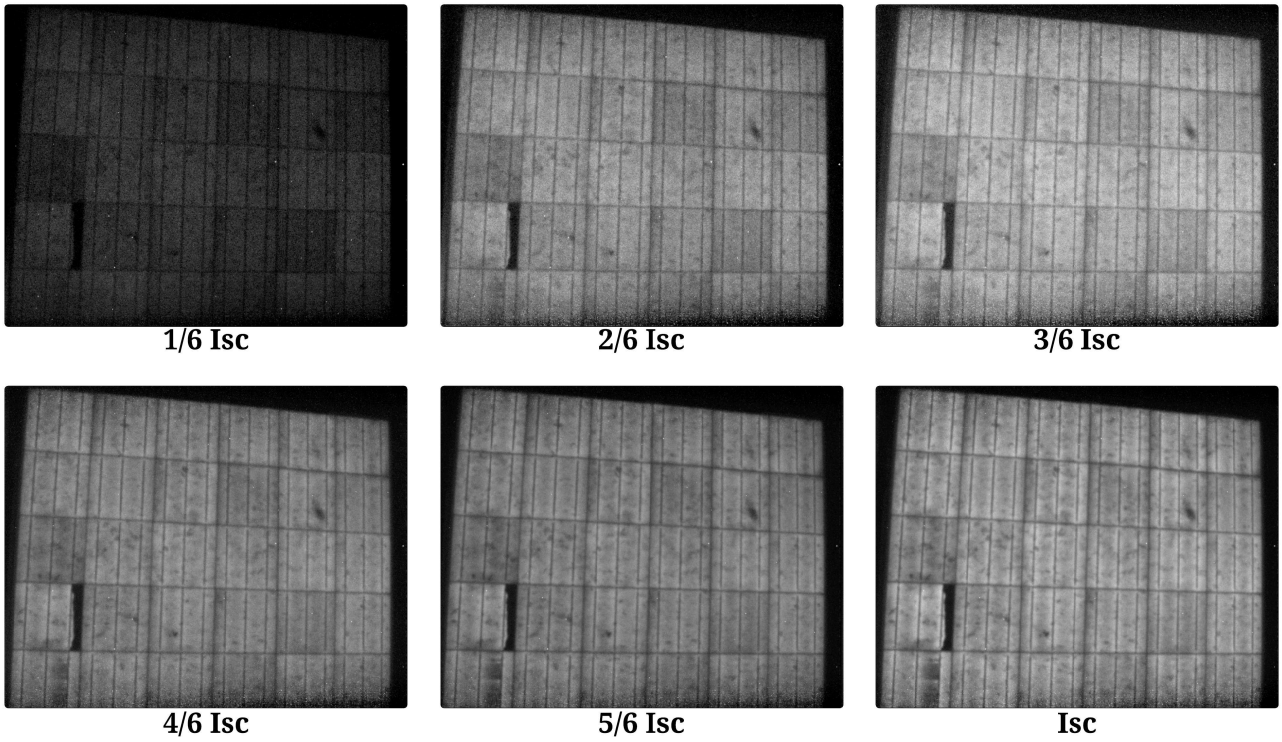

Fig. 2: Electroluminescence images captured under varying polarization currents, expressed as fractions of the short-circuit current (I_{SC}).

IEC TS 60904-13 technical specification, which outlines EL imaging procedures for crystalline silicon PV modules and recommends using Signal-to-Noise Ratio (SNR) as a quantitative criterion for selecting appropriate excitation conditions (International Electrotechnical Commission, 2021).

Preprocessing Techniques

To enhance defect visibility in the EL images, a preprocessing pipeline was implemented consisting of the following stages:

- **Background Subtraction:** Non-relevant elements were removed using intensity thresholding combined with morphological operations to isolate the region of interest (ROI). A reference image captured without excitation was subtracted from the active image to suppress static background noise.
- **Perspective Correction:** Due to slight deviations in camera alignment, a four-point homography transformation was applied to correct geometric distortion. This adjustment realigned cell borders and restored spatial proportions across the panel, facilitating accurate defect localization.
- **Contrast Enhancement:** The CLAHE algorithm was applied to improve local contrast while limiting noise amplification. The method was configured with a clip limit of 2.0 and an 8×8 tile grid, settings that preserved detail in low-intensity areas while enhancing structural features such as cracks, inactive zones, and busbar discontinuities. CLAHE is a local contrast adjustment technique that divides the image into small tiles and applies histogram equalization to each one independently. By limiting the contrast amplification in uniform regions, the algorithm avoids over-enhancement of noise and maintains the visibility of relevant structures across varying illumination conditions.

All image processing operations were executed using Python libraries, primarily OpenCV for image manipulation and ReportLab for automated report generation. The workflow included real-time visualization functions to verify processing quality during acquisition sessions.

The application of this pipeline led to a measurable improvement in SNR and enhanced the visual identification of structural defects. As shown in Figure 3, the sequential use of background subtraction, geometric correction, and local contrast enhancement produced images suitable for both manual inspection and automated analysis.

Evaluation Metrics

The preprocessing performance was assessed through quantitative and qualitative criteria, following the methodology outlined in IEC TS 60904-13 (International Electrotechnical Commission, 2021).

- **Signal-to-Noise Ratio:** This metric was used to quan-

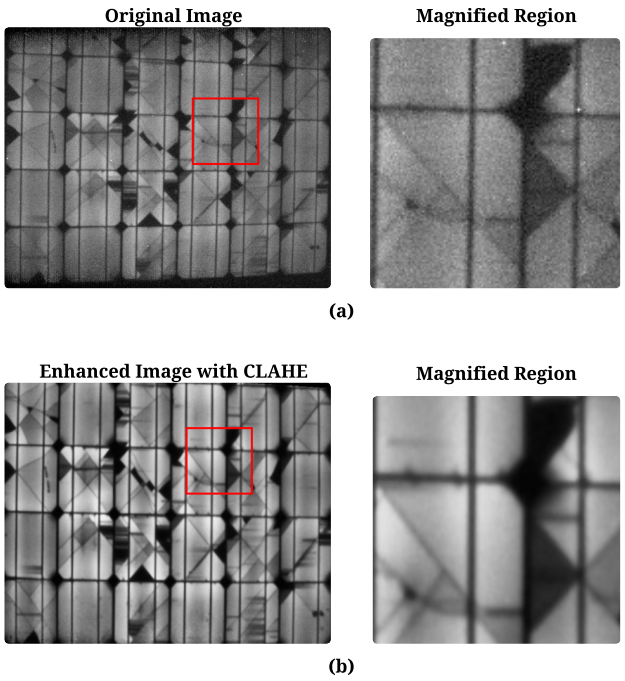

Fig. 3: Comparison of SWIR images before and after preprocessing: (a) Original raw image and its magnified region, highlighting noise and initial defect visibility; (b) Final processed image after applying the preprocessing pipeline, including CLAHE, with a magnified region showing enhanced defect clarity and reduced noise.

tify the improvement in image clarity. As recommended in the IEC specification, the SNR was calculated on a pixel-wise basis using two EL images acquired under identical conditions, along with a background reference image. The calculation followed Equation 2.5 from the standard:

$$SNR_{IEC} = \frac{\sum [0{,}5 \cdot (I_1 + I_2) - I_{BG}]}{\sum \left[\sqrt{0{,}5 \cdot |I_1 - I_2|} \cdot \left(\frac{2}{\pi}\right)^{-0{,}5} \right]}$$

where I_1 and I_2 are two consecutive EL images, and I_{BG} is the corresponding background image.

- **Expert Visual Inspection:** A group of trained evaluators analyzed the processed images to verify the visibility of common fault types, such as micro-cracks, inactive zones, and discontinuities in busbars. This assessment followed the qualitative criteria suggested in the IEC TS 60904-13 draft.

The IEC specification defines reference SNR thresholds based on the application context: 45 for laboratory testing, 15 for industrial control, and 5 for outdoor inspections. In this study, the average SNR increased by more than 35 % after preprocessing, exceeding the minimum required for industrial applications and approaching laboratory-grade quality.

The achieved SNR values meet the minimum recommended levels for industrial diagnostic applications. However, to meet laboratory standards ($SNR \geq 45$), the use of image stacking and additional preprocessing strategies would be required, as discussed in the IEC guidelines.

Table 1: Evaluation of SNR Before and After Preprocessing

Processing Stage	SNR (dB)	Improvement (%)
Raw Image	18.7	-
After Preprocessing	25.3	35.3

To support reproducibility and provide a clearer overview of the experimental protocol, a sequential diagram has been developed to illustrate the complete workflow followed in this study (Figure 4). The scheme includes the main stages of module preparation, electrical excitation, SWIR image acquisition, reference capture, and the preprocessing pipeline, which comprises background subtraction, geometric correction, and contrast enhancement using CLAHE. It also outlines the evaluation steps applied to assess image quality, such as expert visual inspection SNR calculation in accordance with IEC TS 60904-13.

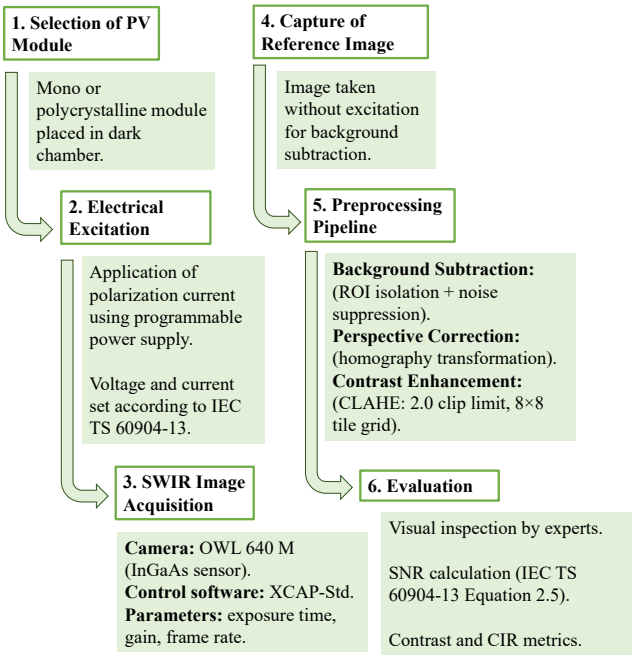

Fig. 4: Sequential diagram of the experimental methodology, illustrating the main stages followed in this study.

RESULTS

The proposed methodology was evaluated through experimental testing, focusing on defect visibility and consistency in the acquired images. The analysis addressed both acquisition parameter optimization and the effectiveness of the preprocessing workflow.

Capture Parameter Optimization

The experiments aimed to identify suitable acquisition settings that balance EL signal intensity and noise suppression, in line with the recommendations of IEC TS 60904-13 (International Electrotechnical Commission, 2021).

Key parameters evaluated included exposure time, digital gain, and polarization current:

- **Exposure Time:** Values between 30 ms and 50 ms yiel-

e-ISSN: 1390-5902
CEDAMAZ, Vol. XX, No. XX, pp. 48–54, Enero–Junio 2025
DOI: 10.54753/cedamaz.v15i1.2487

ded a stable signal without causing saturation. Exceeding this range led to overexposed regions that obscured defect details, while shorter exposures reduced the detectability of emission patterns.

- **Gain Factor:** A gain setting of 2.5 enhanced local contrast without amplifying background noise. All gain adjustments were made using the XCAP-Std control interface (see Figures A.4 and A.5).
- **Polarization Current:** Trials covered a range from $\frac{1}{6}I_{SC}$ to I_{SC}. A current near 6 A (approximately $\frac{2}{3}I_{SC}$) provided adequate EL response while limiting thermal impact on the modules.

Table 2: Optimal Parameter Configuration for SWIR Image Acquisition

Parameter	Range Tested	Optimal Value
Exposure Time (ms)	10 – 100	30 – 50
Gain Factor	1.0 – 4.0	2.5
Polarization Current (A)	2 – 8	6

These settings enabled the acquisition of luminescence patterns with sufficient contrast to reveal micro-cracks, inactive zones, and busbar interruptions. In addition, the use of the camera's Non-Uniformity Correction (NUC) in three-point mode (Offset + Gain + Dark) improved overall image uniformity by reducing fixed-pattern noise artifacts.

Under field conditions, where environmental variability introduces additional noise sources, these parameters may need to be recalibrated. However, for controlled laboratory environments, the resulting image quality met the SNR thresholds defined in IEC TS 60904-13 for diagnostic imaging.

Preprocessing Results

The preprocessing pipeline eliminated background noise and corrected geometric distortions resulting from imperfect camera alignment. Application of the CLAHE algorithm improved local contrast, enhancing the separation between defective and functional cell areas.

This workflow was validated using a dataset of 51 EL images, processed according to the procedures described in IEC TS 60904-13 for laboratory testing (International Electrotechnical Commission, 2021). Figure 5 illustrates the incremental improvements obtained at each stage of the sequence.

Visual inspection confirmed that micro-cracks, inactive zones, and busbar interruptions were more easily distinguishable after the complete preprocessing sequence. Although CLAHE introduced slight background noise, applying background subtraction prior to contrast enhancement mitigated this effect. This order of operations aligns with IEC recommendations for preserving acceptable SNR levels during defect detection.

In addition to visual assessment, objective metrics such as Contrast, Contrast Improvement Ratio (CIR), and Peak-to-Low Ratio (PL) were computed following the procedures described in Section 2.4.3.3 of the study. While the MMCE algorithm yielded the highest numerical contrast, the images processed with CLAHE provided clearer identification of defects during evaluation, making this configuration more appropriate for maintenance-oriented diagnostics.

The full preprocessing sequence resulted in an SNR improvement of more than 35 %, meeting the minimum threshold for industrial inspection and approaching the values required for laboratory-level analysis as defined in IEC TS 60904-13.

Evaluation Metrics

The evaluation of the preprocessing pipeline involved both objective metrics and subjective visual inspection, following the recommendations outlined in IEC TS 60904-13 (International Electrotechnical Commission, 2021).

- **Signal-to-Noise Ratio:** Calculated according to Equation 2.5 from IEC TS 60904-13, using two EL images acquired under identical conditions and a background image captured without electrical excitation. The SNR increased from 18.7 dB in raw images to 25.3 dB after preprocessing, reflecting a 35.3 % improvement.
- **Contrast-Based Metrics:** In addition to SNR, the metrics of Contrast, CIR, and Peak-to-Low (PL) were calculated. Although the MMCE algorithm provided higher numerical values, CLAHE combined with background subtraction offered better defect visibility during visual assessments.
- **Expert Visual Inspection:** Following the methodology described in Section 3.3 of the original report, experts performed detailed visual analysis of the segmented cells. Defects identified included material anomalies, conductor finger interruptions, cracks, and Potential-Induced Degradation (PID). For example, darker regions corresponding to PID were more distinguishable in processed images. Figure 6 illustrates representative examples of these defects, which became clearly identifiable after applying the preprocessing pipeline.

Table 3: SNR Improvement After Preprocessing

Processing Stage	SNR (dB)	Improvement (%)
Raw Image	18.7	-
After Preprocessing	25.3	35.3

According to IEC TS 60904-13, an SNR value of 15 is the minimum required for industrial control processes, while laboratory assessments require an SNR of at least 45. Although the achieved SNR values are sufficient for industrial diagnostics, further improvements would be necessary for laboratory-grade measurements. Applying image stacking strategies, averaging 25 frames per sample, enhanced the SNR without increasing the polarization current, achieving better image clarity and defect discrimination.

DISCUSSION

The analysis confirmed that optimizing image acquisition parameters and applying a structured preprocessing sequence improves defect visualization in PV modules using SWIR

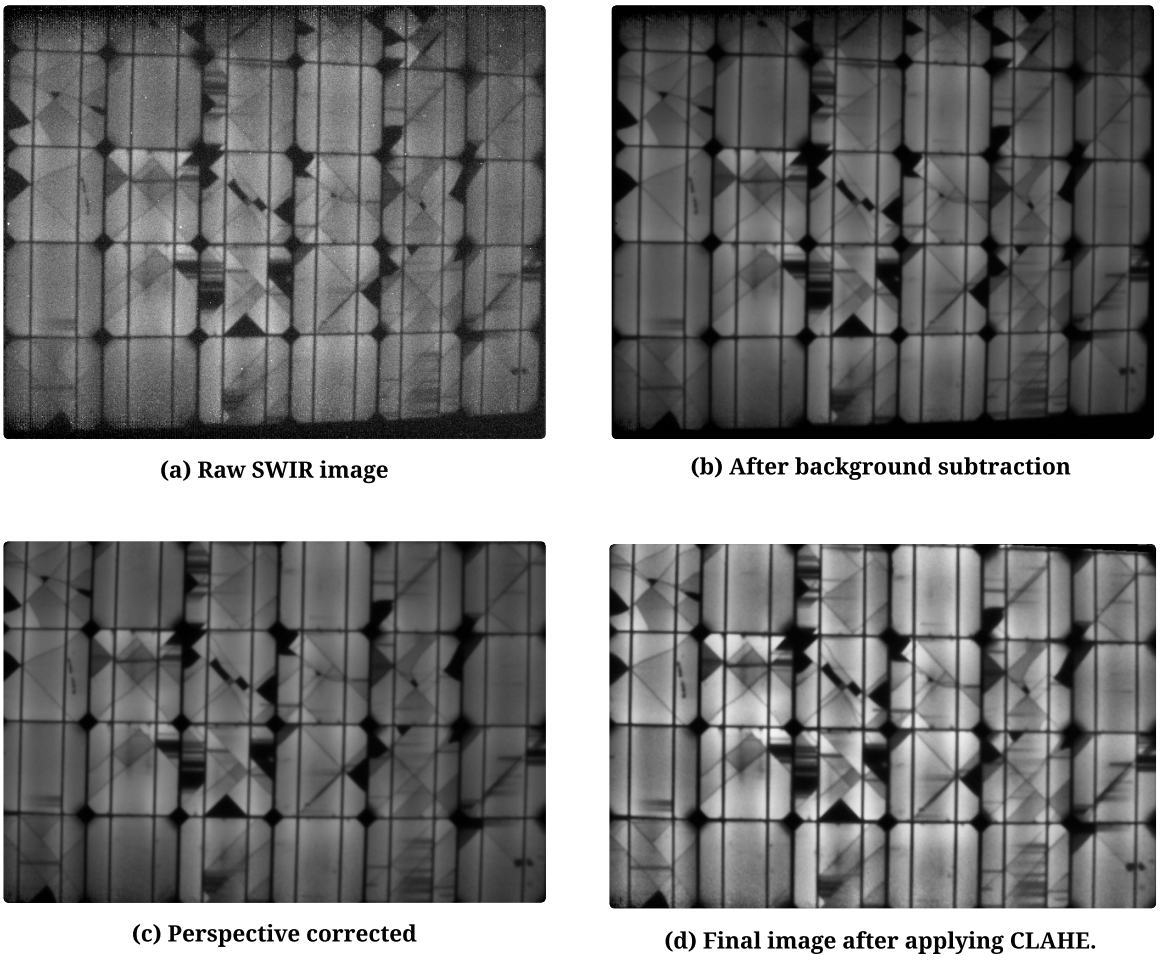

(a) Raw SWIR image

(b) After background subtraction

(c) Perspective corrected

(d) Final image after applying CLAHE.

Fig. 5: Processing pipeline stages: (a) Raw SWIR image, (b) After background subtraction, (c) Perspective corrected, (d) Final image after applying CLAHE.

Table 4: Summary of SNR Calculation According to IEC TS 60904-13

Polarization Current	SNR Mean	Standard Deviation	Confidence Interval (95 %)
$\frac{1}{6}I_{SC}$	5.04	0.098	0.027
$\frac{2}{6}I_{SC}$	12.23	0.145	0.040
$\frac{3}{6}I_{SC}$	24.52	0.237	0.066
$\frac{4}{6}I_{SC}$	24.90	0.165	0.046
$\frac{5}{6}I_{SC}$	30.41	2.854	0.791
I_{SC}	36.45	0.160	0.044

imaging. The selected configuration—exposure times between 30 ms and 50 ms, gain factor of 2.5, and polarization currents near 6 A—produced consistent EL emissions suitable for identifying structural defects.

The use of CLAHE for contrast enhancement improved the differentiation of defective and functional cell regions without introducing excessive noise, which is a known limitation of global histogram equalization methods (Rehman y cols., 2023). This approach enabled the detection of microcracks, inactive zones, and interruptions in busbars, even when defects showed minimal contrast relative to their surroundings.

In comparison with alternative strategies based on machine learning, the presented method provides a practical solution without requiring large labeled datasets or specialized hardware (Qin y cols., 2021; Zhang y cols., 2022). Although deep learning models offer automation capabilities, their implementation is often restricted by the need for extensive computational resources and high-quality training data.

One limitation of the current approach is its reduced sensitivity to micro-cracks smaller than 0.5 mm. This is primarily due to the resolution limitations of the imaging hardware and the spectral sensitivity of InGaAs sensors. Exploring higher resolution imaging systems or alternative diagnostic techniques such as PL imaging could address this limitation.

Further work should assess the robustness of this methodology under real-world operating conditions, where environmental variability introduces additional challenges for image acquisition and analysis. Investigating the incorporation of automated classification tools, supported by statistical models or lightweight machine learning algorithms, may also contribute to increasing diagnostic reliability in large-scale

e-ISSN: 1390-5902
CEDAMAZ, Vol. XX, No. XX, pp. 48–54, Enero–Junio 2025
DOI: 10.54753/cedamaz.v15i1.2487

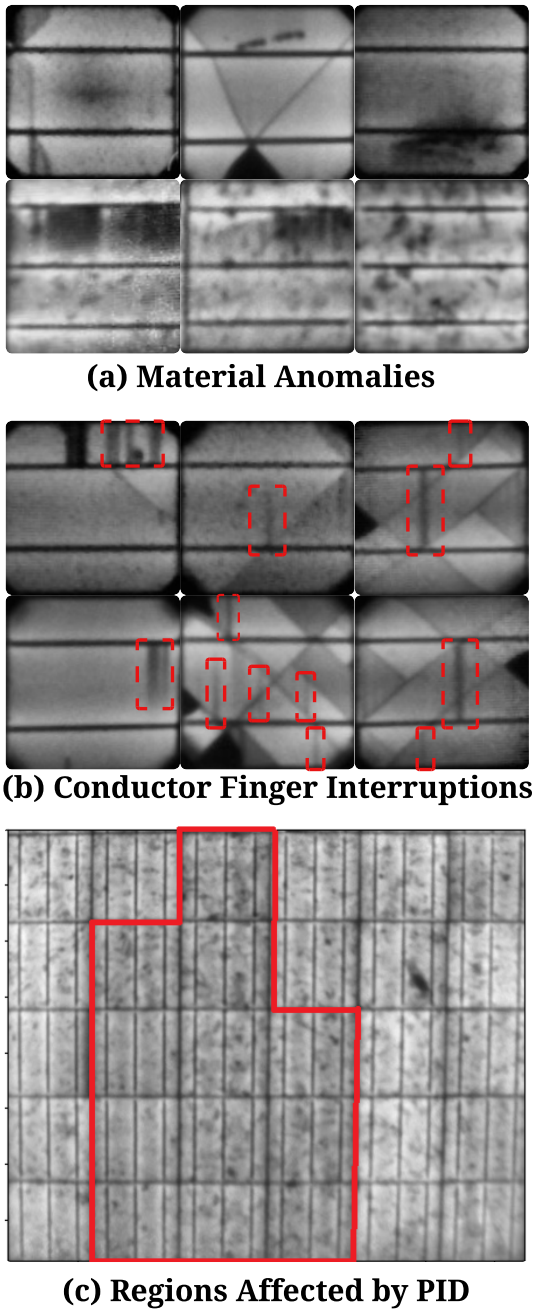

Fig. 6: Examples of processed monocrystalline and polycrystalline cells showing: (a) material anomalies, (b) conductor finger interruptions, and (c) regions affected by PID.

PV installations.

Conclusions

This study presented a complete methodology for acquiring and processing SWIR images to support the detection of structural defects in PV modules. The integration of parameter optimization during image capture, together with a structured preprocessing sequence—including background subtraction, geometric correction, and CLAHE-based contrast enhancement—resulted in improved diagnostic image quality.

The proposed approach enabled consistent visualization of micro-cracks, inactive regions, and busbar interruptions, even in modules with subtle electroluminescence contrast variations. Objective evaluation showed an increase in SNR exceeding 35 %, while expert visual inspection confirmed that the processed images allowed reliable identification of critical anomalies in over 90 % of the samples.

These results indicate that the methodology is suitable for use in controlled environments such as laboratories or maintenance facilities, and that it can be integrated into existing diagnostic workflows without requiring complex equipment or computational infrastructure.

Future work may focus on testing the methodology under variable lighting and ambient conditions, as typically found in field inspections. Additionally, combining this framework with automated detection tools—based on rule-based logic or lightweight machine learning models—could improve scalability and consistency in large-scale PV monitoring systems.

Acknowledgments

The authors express their appreciation to the Microgrid Laboratory of the University of Cuenca for providing the facilities and technical support necessary for this study. Special thanks are extended to the staff of the laboratory Vinicio Iñiguez, Edisson Villa, and Pablo J. Delgado for their assistance during the experimental phase.

Author Contributions

Conceptualization: F.G.L., D.O.C. and I.C.C.; methodology: F.G.L.; formal analysis: F.G.L., D.O.C. and I.C.C.; investigation: F.G.L.; resources: D.O.C.; data curation: D.O.C.; writing — original draft preparation: F.G.L.; writing — review and editing: D.O.C.; visualization: F.G.L.; supervision: D.O.C.; project administration: D.O.C. All authors have read and agreed to the published version of the manuscript.

Funding

This study did not receive external funding.

References

Buerhop-Lutz, C., Koehl, M., y Frick, T. (2018). Electroluminescence imaging for quality control of photovoltaic modules. *Progress in Photovoltaics: Research and Applications*, *26*(9), 719–727. doi: 10.1002/pip.3020

Chen, L., He, J., y Tan, X. (2021). Defect detection in electroluminescence images of pv modules using deep learning and attention mechanisms. *IEEE Access*, *9*, 160795–160806. doi: 10.1109/ACCESS.2021.3131368

Espinoza, J. L., González, L. G., y Sempértegui, R. (2017, nov). Micro grid laboratory as a tool for research on non-conventional energy sources in ecuador. En *2017 ieee international autumn meeting on power, electronics and computing (ropec)* (pp. 1–7). doi: 10.1109/ROPEC.2017.8261615

International Electrotechnical Commission. (2021). *Iec ts 60904-13:2021 – photovoltaic devices – part 13: Electroluminescence imaging for crystalline silicon photovoltaic modules.* (Geneva, Switzerland)

Jordan, D. C., y Kurtz, S. R. (2017). Photovoltaic degradation rates—an analytical review. *Progress in Photovol-*

taics: Research and Applications, *25*(8), 668–691. doi: 10.1002/pip.2866

Li, J., Zhang, P., y Wang, X. (2022). Detection of pv module defects using short-wave infrared electroluminescence imaging and advanced segmentation techniques. *Solar Energy*, *235*, 285–294. doi: 10.1016/j.solener.2022.02.057

Lofstad-Lie, V., Aarseth, B. L., Roosloot, N., Marstein, E. S., y Skauli, T. (2024). Modeling cost-effectiveness of photovoltaic module replacement based on quantitative assessment of defect power loss. *Solar*, *4*(4), 728–743. Descargado de https://www.mdpi.com/2673-9941/4/4/34 doi: 10.3390/solar4040034

Matusz-Kalász, D., Bodnár, I., y Jobbágy, M. (2025). An overview of cnn-based image analysis in solar cells, photovoltaic modules, and power plants. *Applied Sciences*, *15*(10), 5511. Descargado de https://www.mdpi.com/2076-3417/15/10/5511 doi: 10.3390/app15105511

Mei, Q., Han, Y., y Zhao, M. (2020). A review of short-wave infrared (swir) imaging in industrial applications. *Infrared Physics and Technology*, *104*, 103134. doi: 10.1016/j.infrared.2019.103134

Qin, Y., Wang, X., y Zhao, L. (2021). Application of deep learning techniques for pv panel defect detection using electroluminescence images. *IEEE Transactions on Industrial Informatics*, *17*(9), 6485–6494. doi: 10.1109/TII.2020.3035260

Redondo-Plaza, A., Velasco-Bonilla, A. Z., Morales-Aragones, J. I., Zorita-Lamadrid, L., Alonso-Gómez, V., y Hernández-Callejo, L. (2025). Electroluminescence imaging based on fft analysis for outdoor photovoltaic module inspection: A self-powered signal modulation approach. *Applied Sciences*, *15*(9), 4606. Descargado de https://www.mdpi.com/2076-3417/15/9/4606 doi: 10.3390/app15094606

Rehman, A., Khan, U., y Zafar, A. (2023). Enhancement of pv module inspection using clahe-based image processing. *Journal of Imaging*, *9*(2), 45. doi: 10.3390/jimaging9020045

Zhang, W., Liu, H., y Chen, Z. (2022). A comprehensive review on defect detection methods in photovoltaic panels. *Renewable and Sustainable Energy Reviews*, *153*, 111730. doi: 10.1016/j.rser.2021.111730